INTERNATIONAL ATOMIC ENERGY AGENCY
UNITED NATIONS EDUCATIONAL, SCIENTIFIC AND CULTURAL ORGANIZATION
INTERNATIONAL CENTRE FOR THEORETICAL PHYSICS
I.C.T.P., P.O. BOX 586, 34100 TRIESTE, ITALY, CABLE: CENTRATOM TRIESTE

SMR.769 - 3

WORKSHOP ON "NON-LINEAR ELECTROMAGNETIC INTERACTIONS IN SEMICONDUCTORS"

1 - 10 AUGUST 1994

"Optical Second Harmonic Generation Study of Semiconductor Interfaces"

T. RASING
Department of Physics
University of Nijmegen
Toernooiveld 1
NL-6500 GL Nijmegen
THE NETHERLANDS

Contribution to:
Nonlinear Electromagnetic Interactions in Semiconductors.

Lecture Notes Trieste, August 1994

Optical Second Harmonic Generation Study of Semiconductor Interfaces

Theo Rasing
Research Institute for Materials
University of Nijmegen
NL - 6525 ED Nijmegen, The Netherlands

Optical Second Harmonic Generation (SHG) has been shown to be a very sensitive probe to investigate the symmetry and electronic structure of semiconductor surfaces and interfaces. Applications to surface reconstructions, step structure and epitaxial growth have been proven very successful. However, as an optical techique, SHG is particularly attractive to probe buried interfaces, that are hardly accessible otherwise. In these lectures, the basic principles of SHG for interface studies will be discussed and illustrated with a number of applications. Two important examples are the $Si - SiO_2$ interface and the $GaAs - Au$ interface, the latter as an example of the general problem of the electronic properties of a Schottky barrier.

Contents

1 Introduction.

With the development of artificial structures like quantum wells or dots and the still continuing trend to smaller devices, the role of the surfaces and interfaces is becoming increasingly important[1]. In parallel, one has observed a strong development in surface science techniques in the past decades, resulting in the ultimate atomic resolution of the Scanning Tunneling Microscope (STM)[2]. However, many important fundamental and practical problems are concerned with buried interfaces, that are practically inaccessible by most surface science techniques that rely on either electron or ion scattering[3]. Examples are semiconductor-oxide and semiconductor-metal (Schottky barrier) interfaces.

Recently, second order nonlinear optical techniques like Second Harmonic Generation (SHG) and Sum Frequency Generation (SFG) have been developed as extemely versatile and sensitive surface and interface probes[4, 5]. Optical surface probes have some definitive advantages: they are applicable to any interface accessible by light, while the use of ultra short laser pulses leads to an unprecedented time resolution. However, usually optical techniques lack the necessary surface specificity and sensitivity. SHG and SFG derive their surface sensitivity from the symmetry breaking at interfaces. As will be shown below, this simple symmetry argument can lead to powerful applications.

SHG arises from the nonlinear polarization $\vec{P}(2\omega)$ induced by an incident laser field $\vec{E}(\omega)$.

$$P_i(2\omega) = \chi^{(2)}_{ijk} E_j(\omega) E_k(\omega) \tag{1}$$

where $\chi^{(2)}$ is the second order susceptibility tensor reflecting the structure and symmetry properties of the system. Eq.1 shows that for a system with inversion symmetry, $\chi^{(2)}$ must be identical zero, except at interfaces where this symmetry is necessarily broken. This is the origin of the surface sensitivity of SHG (and similarly SFG). The nonlinear polarization $\vec{P}(2\omega)$ leads to an SHG intensity $I(2\omega)$ given by[6]:

$$I(2\omega) = C|\hat{e}_{2\omega} \stackrel{\leftrightarrow}{\chi}^{(2)} \hat{e}_\omega \hat{e}_\omega|^2 I(\omega)$$

with $\hat{e}_i$ the polarization vectors of the fundamental and harmonic frequencies, $I(\omega)$ th pump intensity and C a frequency dependent constant determined by a full solution of the Maxwell equations and boundary conditions. The small nonlinear surface signals require the high peak powers of pulsed lasers. As an example, we consider the SHG from a $Si(111)$ surface. With a laser excitation at 1.06 μm from a Q-switched $Nd-YAG$, producing $8ns$ pulses at 10 Hz repetition rate, a pump energy of 10 mJ in a 1 mm diameter spot generates about 10^3 photons per pulse at the harmonic frequency. Though this is easily detectable by modern photon counting techniques, this example corresponds to an efficiency $\eta = I(2\omega)/I(\omega)$ of about 10^{-14}. This means that for surface and interface SHG experiments, special attention has to be adressed to the frequency filtering and suppression. On the other hand, as 2ω and ω are well separated, high resolution in frequency is

not required. Fig. 1.1 shows a typical experimental configuration, with a sample mounted on a rotation stage in air.

The next order nonlocal term of the nonlinear polarization can be written as

$$\vec{P} = \overleftrightarrow{\chi}^{(2)}_{NL} \vec{E} \bigtriangledown \vec{E} \tag{2}$$

where $\overleftrightarrow{\chi}^{(2)}_{NL}$ is a fourth rank tensor. Though such gradient terms are a factor kd smaller than the surface term (k = optical wave vector and d = atomic dimension-surface layer thickness), the bulk contribution originates from a layer of thickness $\sim k^{-1}$ in comparison with a surface contribution of a layer thickness d. This means that for the surface to bulk ratio

$$\frac{I_s}{I_B} \sim \left| \frac{\chi_s d}{\chi_B k^{-1}} \right|^2 \sim \left| \frac{\chi_s d}{k d \chi_s k^{-1}} \right|^2 \sim 1 \tag{3}$$

This rough estimate indicates that surface and bulk could equally contribute to the total SHG response. This is important to realize for the application of SHG to surface and interface studies. An additional complication is that the various bulk terms radiate as an effective surface term, so that both contributions cannot easily be separated[4]. Experimentally, this can sometimes be done by altering the surface contribution, for example by chemical modification (oxidation), or by polarization selection, when surface and bulk have different symmetries. An example is shown in Fig 1.2, showing the effect of oxidation on the SHG response from a clean, reconstructed $Si(111)$ surface[7]. These results clearly show that for a clean $Si(111)$ crystal, the SHG response is dominated by the surface. The dangling bonds on the clean surface (see Fig. 1.3) are responsible for this high nonlinear response, that is quenched when oxygen is adsorbed on these bonds.

Apart from the surface/bulk discrimination, the important point is what can be learned from this technique. The physical parameter that contains all the information of the system of interest is the nonlinear susceptibility tensor $\overleftrightarrow{\chi}^{(2)}$. $\overleftrightarrow{\chi}^{(2)}$ will depend on

1) interface symmetry and geometrical structure

2) interface electronic structure

By proper selection of input and output polarizations, various $\chi^{(2)}$ compounds can be determined. Being a third rank tensor $\overleftrightarrow{\chi}^{(2)}$ in principle has 27 elements. Though symmetry will reduce this number drastically in most cases, still there will generally be many nonzero elements that contain information about the system of interest. Table I shows the nonvanishing elements of the surface $\chi^{(2)}_s$ for surfaces of various symmetry. A nice comparison with linear optics can be seen in Fig. 1.4, showing the anisotropy in the SHG from a $Si(111)$ wafer. Whereas the linear reflection from this sample is purely isotropic, the SHG results clearly display the 3-fold symmetry of this surface.

This sensitivity to surface symmetry and symmetry changes can be used in a very interesting way. Fig. 1.5 shows the change in SHG signal from a $Si(111)$ surface as a function of temperature. The data are from a clean, 7×7 reconstructed surface, that undergoes a transition to a 2×1 reconstruction at about $550°K$. As these two reconstructions have different symmetries and therefore different surface $\chi^{(2)}$ components, SHG can here be used to monitor this surface phase transition in situ![11]
The examples above have shown the intrinsic surface sensitivity of optical SHG. Yet for future studies, the most interesting applications are the investigation of buried interfaces and the exploitation of the intrinsic high time resolution that is offered by using a pulsed laser technique. A few of such applications will be adressed in the following chapters.

symmetry classes	location of mirror plane	independent nonvanishing elements
C_1	no mirror	xxx, xxy=xyx, xyy, yxx, yxy=yyx, yyy, xxz=xzx, xyz=xzy, yxz=yzx, yyz=yzy, zxx, zxy=zyx, zyy, xzz, yzz, zxz=zzx, zyz=zzy, zzz
C_{1v}	$x - z$	yyx=yxy, xyy, xxx, yyz=yzy, xxz=xzx zxx, zyy, xzz, xzz, zxz=zzx, zzz
C_{2v}	$x - z$, $y - z$	xxz=xzx, yyz=yzy, zxx, zyy, zzz
C_{3v}	$x - z$	xxx=-xyy=-yyx=-yxy, zxx=zyy, xxz=xzx=yyz=yzy, zzz
C_{4v}, C_{6v} or isotropic	$x - z$, $y - z$	xxz=xzx=yzy=yyz, zxx=zyy, zzz

Table 1: *Independent nonvanishing elements of* $\bar{\chi}(2\omega)$ *for surfaces of various symmetry classes (surfaces in the* $x - y$ *plane)*

2 SHG studies of the structure of vicinal $Si(111)$ and $Si(110)$ surfaces.

Vicinal or stepped surfaces are important for applications in epitaxial crystal growth. They are obtained by cutting a crystal under a small misfit angle relative to the surface normal. The resulting structure shows flat terraces, of the original surface plane, separated by steps[8]. The average step density is determined by the miscut angle. Fig. 2.1 shows a schematic picture of a vicinal $Si(111)$ surface, including the 3 mirror planes of the (111) terraces. At the steps, only the mirror plane (m_1) perpendicular to the steps survives.

The vicinal $Si(111)$ samples were cut with a small offset angle θ in the $(11\bar{2})$ directon and covered with a native oxide. Fig. 2.2 shows the observed angular dependence of the s- and p- polarized SHG for s-polarized excitation. The reflected SHG was recorded while the samples were rotated around the surface normal as schematically shown in the figure.

The top traces (for $\theta = 0°$) are in perfect agreement with the C_{3v} symmetry of $Si(111)$. They are described by[9]:

$$E_{ss}(2\omega) \sim A \sin 3\psi \tag{4a}$$

$$E_{sp}(2\omega) \sim B + C \cos 3\psi \tag{4b}$$

The data for the vicinal surfaces ($\theta = 3°$ and $5°$) show an interference between the original C_{3v} symmetry (of the terraces) with a C_{1v} symmetry (of the steps). The latter contribution increases with increasing offset angle i.e. increasing step density. This shows that SHG is not only sensitive to the surface symmetry, but can also detect the presence of (a regular pattern) of steps, allthough the latter only have a height of 3.14 Å in this case.

An even more striking example is shown in Fig. 2.3, displaying the reflected SHG from a flat and vicinal $Si(110)$ surface. This (110) surface has an average C_{2v} symmetry, yielding a zero anisotropic surface contribution. As a result, $E_{ss}(2\omega)$ can only originate from the bulk and appears to be nearly zero. On the other hand, the signal from the vicinal surface is very strong and is a pure step contribution, showing the expected C_{1v} symmetry[10]. In this case, SHG can also yield more microscopic information about the step structure. A real interface never has perfectly straight steps, but rather displays kinks, as schematically shown inf Fig. 2.4. The different bound orientations at the step edges and kinks lead to different contributions to the macroscopic $\chi^{(2)}$ tensor. From such a microscopic model one can deduce from the SHG data that in this case, the kink density was about 4% (see Fig. 2.5)

3 SHG studies from thick thermal oxides on $Si(111)$.

3.1 Introduction.

Silicon dioxide is an extremely important material for microelectronics. With the move to thinner oxides, grown at lower temperatures, the oxide quality has become more important, especially in relation to electrical breakdown[12]. The structure of the silicon/oxide interface, in particular its roughness and stoichiometry appears to play an important role in this. Many observations suggest that there is a difference between the oxide near the interface and the oxide more further away. Possibilities of strained and even crystalline oxide layers have been suggested (see Fig. 3.1).

Recently a number of Second Harmonic Generation (SHG) experiments have been performed on (thick) oxide films on silicon to study the possible presence of strain, crystalline SiO_2, static electric field and roughness at the Si-SiO_2 interface. Large enhancements of the SHG anisotropy have been observed on thick oxide films. To apply SHG as a quantitative probe for these technologically important interfaces, the question to be adressed is: what are the sources of the observed nonlinear signal. It will be shown here that the SHG on thick thermal oxide films on Si(111) as a function of oxide thickness and angle of incidence is dominated by linear optics, due to multiple reflections in the oxide film.

For a flat Si(111) surface the s-polarized SHG field for s-polarized exitation $E_{s,s}$ can effectively be characterized by one response parameter χ, and the reflected SH intensity $I_{s,s}$ can be written as:

$$I_{s,s}(2\omega) \sim L_{2\omega} \mid \chi \mid^2 L_\omega^2 I^2(\omega) \sin(3\psi) \tag{5}$$

Here $I(\omega)$ is the pump intensity, and L_ω and $L_{2\omega}$ are the linear Fresnel factors at ω and 2ω respectively. The wavevectors for the fundamental and SH field are matched by the nonlinear boundary condition [6]:

$$k_\parallel(2\omega) = 2k_\parallel(\omega) \tag{6}$$

For Si(111)-SiO_2 this model is consistent with SHG contributions from the silicon bulk, the Si-SiO_2 interface and a possible SiO_x or crystalline SiO_2 transition layer. It does exclude contributions from the SiO_2 bulk, as is expected for a centrosymmetric medium with low nonlinear response. It also excludes contributions from the SiO_2-air interface, which is experimentally verified by the abscence of isotropic contributions to $I_{s,s}$, as was also observed in a number of other experiments on oxidized Si(111)[9, 13, 14, 15].

For an oxide film on a silicon substrate no extra contributions to the SHG are expected, in contrast to some recent observations that report a distinct effect of the oxide thickness on the SHG [17, 18]. It can easily be shown that these observations are mostly due to interference effects in the oxide layer, that have to be taken into account before discussing any other possible nonlinear sources.

Having a refractive index between that of air and silicon and negligible absorption for wavelengths from the UV to the infrared, an oxide film on silicon can act as a resonator that can enhance the coupling of the fields into and out of the silicon. Describing such films with a perfect 3-layer model (air-SiO_2-Si), it is straightforward to write down the Fresnel factors L_ω and $L_{2\omega}$ [21]. For an incoming field in air at frequency ω and a certain oxide thickness, the field at the Si-SiO_2 interface just inside the silicon is calculated and matched to the field at 2ω by using Eq. 6. For this SHG field at the interface the transmission to the air is then calculated. Thus for a given χ of the Si-SiO_2 interface and Si bulk, the dependence of $I_{s,s}$ on the angle of incidence and oxide thickness is completely described. Of course such a model can be extended to include more interfaces which do have an SHG response [22, 23].

3.2 Results and Discussion

Fig. 3.2 shows the amplitude of $I_{s,s}$ as a function of angle of incidence for oxide thicknesses of 310 (circles) and 260 nm (triangles), and for the reference sample with a natural oxide (squares). All data are plotted on the same scale. The reference sample shows the characteristic monotonic decay from a maximum at 0° to zero at 90° [16, 19, 20]. Of course, multiple reflections play a minor role for this thin oxide. Taking for Si $n(\omega)= 4.151+i0.052$ and $n(2\omega)=1.854+i4.438$ [24], the measurement is well described by our multiple reflections model (solid line). The measurements on the thick oxides show a large increase in SHG. Although the overall angle dependence is similar as for the natural oxide, now maxima appear at 25° (310nm) and 55° (260nm). For both thicknesses the azimuthal dependence contained only an anisotropic term, so no contribution from the oxide, which would be isotropic. Taking for SiO_2 $n(\omega)=1.461$ and $n(2\omega)=1.500$ [25], and using the same scaling parameter for both curves, the measurements are very well described by the multiple reflections model, both in amplitude and angle dependence. The dotted line is the prediction from this model for a 2nm oxide, given the amplitudes for 310nm and 260nm. It shows that the χ parameter of the thermal oxide is a factor 1.2 larger than that of the natural oxide. This difference indicates that these are two different interfaces, and shows that SHG could be used to study the microscopic differences between thermal and natural silicon oxides.
A likely interpretation of this observed difference can be given as follows. A less perfect interface leads to a partial destruction of the coherence between the microscopic contributions of the $Si-Si$ and $Si-O$ bonds to the macroscopic $\chi^{(2)}$, leading to a smaller $\chi^{(2)}$. This means that the interface of the thermal oxide has a higher quality.
The appearance of a maximum in the angular dependence can be understood in terms of the optical pathlength in the oxide film. For every oxide thickness there is an angle of incidence such that the multiple reflected fields interfere constructively at the Si-SiO_2 interface, leading to a higher field in the silicon and a higher SH response. For the generated SH field the argument is analogous.
This thickness dependence is more directly demonstrated in Fig. 3.3, where the amplitude of $I_{s,s}$ (dots) and linear reflection (squares) are plotted as a function of oxide thickness, at an angle of incidence of 4°. These data clearly show oscillations that are described very

well by this multiple reflections model (solid lines). The linear Fresnel factors L_ω and $L_{2\omega}$ show interference. Neglecting the difference in phase rotation upon reflection from silicon (which is negligible for the fundamental field at 532nm, but not for the SH field) and the dispersion in the oxide, the period for $L_{2\omega}$ would be exactly twice that of L_ω. Because of the phase rotation and the dispersion in the oxide, the curve for $L_{2\omega}$ shifts and its period is no longer exactly half of that for L_ω. Thus the phase rotation leads to a shift of the interference peaks and the dispersion leads to a gradual change of the peakheights. One can calculate that a maximum enhancement of $I_{s,s}$ at an angle of incidence of 4° is obtained for an oxide thickness of ~1200nm. The open symbols at 2nm are measured on a part of the sample that was etched clean and then put in air, to attain a thin natural oxide again. These data are well described by the model curves for both the SHG and the linear reflectance. This means that the thermal oxide and the natural oxide obtained after etching the thermal oxide away actually have the same SHG response parameter χ. This suggests that these two interfaces are the same or that SHG is insensitive to the differences between them. Contrary to the example of Fig. 3.2 for a natural oxide of unknown history, in this case the results at 2nm are completely consistent with the thick oxides.
The changes in $I_{s,s}$ can thus be completely understood in terms of multiple reflections in the oxide film. The analysis is simplified by the fact that for this polarization the SHG can effectively be characterized by one single parameter. The same applies to the s-polarized SHG for a p-polarized pump field, which also only contains anisotropic contributions.
For the p-polarized SHG both isotropic and anisotropic contributions arise, and the number of contributing tensor elements increases. The SHG can then no longer be characterized by a single parameter χ. However, from Snell's law it follows that if only multiple reflections play a role, with no other SHG source, only the amplitude of the electric field changes, not the p/s-polarization ratio. This would imply that also for $I_{p,p}$, the anisotropy scales with oxide thickness. $I_{p,p}$ hase been measured as a function of angle of incidence on the sample with 310nm and 260nm oxide thickness and on the reference sample. The results can be described by [13, 20]:

$$E_{p,p}(2\omega) = \mathrm{A} + \mathrm{B}e^{i\Phi}\cos(3\psi), \tag{7}$$

where A is the isotropic and B the anisotropic contribution, both containing several bulk and surface tensor elements that have different angle of incidence dependences, and Φ is the phase difference between A and B. In Fig. 3.4 the ratio A/B is plotted for all three measurements. Note first that for all samples the ratio A/B is indeed not constant. For the reference sample (squares) the ratio A/B=1 at an angle of incidence of 45°, in agreement with a number of experiments on Si(111) in air [13, 14, 15, 9]. For 310nm (circles) and 260nm (triangles) the ratio A/B is the same as for the reference sample up to 45°, after which they clearly deviate. These results suggest that there is an extra SHG source. These could be trapped charges at the interface giving rise to a symmetry breaking DC-electric field. This point will be further adressed in a more extensive study.
In conclusion the effect of a thick oxide layer on the SHG from thermally oxidized Si(111) is dominated by linear optics, due to multiple reflections in the oxide film. These multiple reflections can enhance the SHG significantly when compared with a natural oxide sample

and are not related to any SHG source in the oxide itself, as was suggested before [17, 18]. For the s-polarized SHG this leads to an overall scaling of the anisotropy, which contains only anisotropic contributions. For the p-polarized SHG however, the form of the anisotropy is also changed, suggesting an extra SHG source. For natural oxides of 2nm one can of course neglect the effects of multiple reflections. However, for these natural oxides, the SHG appears to depend on the sample preparation. These measurements show that one should be carefull in analyzing the SHG from a buried interface, and take into account the possibility of multiple reflections in the overlayer.

4 SHG studies of $GaAs - Au$ interfaces.

4.1 Introduction.

The problem of Schottky barrier formation at a metal- semiconductor interface still attracts a lot of attention, as new developments in material fabrication and structure determination have shown that the precise interface structure plays a crucial role in determining the Schottky barrier height . For electro- optic applications, not only the static electronic structure but even more importantly, the dynamics near these interfaces is extremely relevant, as this will affect the speed of such devices. Recent photoluminescence studies of a Au/GaAs structure have shown unexpected field and laser intensity dependences at quite moderate laser powers (10 mW) that are commonly met in optical semiconducting devices [26, 27]. Theoretical models suggest a very rapid drop of the effective barrier height as a result of the spatial separation of the carriers excited by the incident laser puls (carrier sweepout). The physics of this problem is schematically illustrated in Fig. 4.1a. Fig. 4.1b shows the behaviour of the effective Schottky barrier field, as found from Monto Carlo simulations. However, the photoluminescence is only indirectly affected by this interface field, as the signal is coming from a large bulk region. Very recently, Qi et al [28] showed the power of SHG to probe the band bending region in GaAs. A direct way to probe the (time evolution of the) effective Schottky barrier height would be to measure the field induced SHG with ultra short excitation pulses.

4.2 SHG at a metal-semiconductor interface.

For an incident electric field $\vec{E}(\omega)$ the reflected SHG-field follows from the nonlinear polarization $\vec{P}(2\omega)$. In the electric dipole approximation $\vec{P}(2\omega)$ is related to $\vec{E}(\omega)$ and an applied dc electric field $\vec{E}_{SB}(0)$ via nonlinear susceptibility tensors as:

$$\begin{aligned} \vec{P}(2\omega) &= \left(\chi_S^{(2)} + \chi_B^{(2)}\right) : \vec{E}(\omega)\vec{E}(\omega) \\ &+ \left(\chi_S^{(3)} + \chi_B^{(3)}\right) : \vec{E}(\omega)\vec{E}(\omega)\vec{E}_{SB}(0) \end{aligned} \tag{8}$$

where χ_S and χ_B are the interface and bulk nonlinear susceptibility tensors, respectively. Since GaAs has no inversion symmetry there are both bulk and interface nonzero tensor elements. The GaAs(100) surface has 4mm symmetry, and the three independent nonzero interface susceptibility elements are $\chi^{(2)}_{S;zzz}$, $\chi^{(2)}_{S;zii}$ and $\chi^{(2)}_{S;izi}$ with $i = x,y$[6, 29]. For the bulk of the 43m symmetric GaAs(100) crystal there is only one independent nonzero susceptibility element $\chi_B^{(2)} = \chi^{(2)}_{B;ijk}$ with $i \neq j \neq k$[29]. The subscripts (i,j,k) refer to the principal axes (x,y,z) of the cubic crystal, with z along the interface normal. The second term in equation 8 describes the so called electric field induced second harmonic generation.
This field $\vec{E}_{SB}(0)$ has only a z-component, which we will indicate with E_{SB}. The fourth rank tensors in the second term of equation 8 reduce to third rank tensors, when multiplied with E_{SB}, and have the same nonzero elements as the tensors $\chi_S^{(2)}$ and $\chi_B^{(2)}$[28].

The maximum static electric field E_{SB} at the SB is calculated from the well known equation[30]

$$|E_{SB}(z=0)| = \left(\frac{2qN_D\Phi_b}{\epsilon_0\epsilon_S}\right)^{1/2} \tag{9}$$

where N_D is the doping density, ϵ_0 is the dielectric permittivity, ϵ_S is the static dielectric constant, and Φ_b is the bandbending at the interface. The latter is given by: $\Phi_b = \Phi_{b0}+V_b$. Φ_{b0} is the bandbending when no biasvoltage is applied and V_b is the value of an applied reversed bias voltage.
The Schottky barrier sample we used for our experiments, is grown on a n+ GaAs substrate. The actual barrier is formed by an 0.3 μm-thick n-type GaAs (doping concentration: 10^{17} cm^{-3}) layer and a semi-transparant Gold film of 80 Å-thickness, to allow for laser excitation through the metal top contact. Further details on the sample can be found in [26]. A voltage bias can be applied across the sample between an AuGeNi backside-contact and the top contact. Capacitance-voltage measurements indicate a value for the Schottky barrier height of 0.90 V.
The pump radiation for the SHG measurements was supplied by a mode-locked Titanium Sapphire laser that operated at λ = 770 nm and produced trains of 70 fs pulses at a 82 MHz repetition rate. The photon energy at this wavelength is 1.61 eV; this is above the bandgap of GaAs, which is 1.43 eV at room temperature; The sample was subjected to pump radiation at 45° angle of incidence. The diameter of the spot was about 100 μm.

4.3 Results and discussion

Figure 4.2a shows half of the azimuthal anisotropy for two different bias voltages and an average laser power of 4 mW. Figure 4.2b shows the same, measured with an average laser power of 19 mW. The open circles present data at 0 V bias, the dots at -4 V. Figure 4.2a shows a very clear bias dependence of $I_{2\omega}$, that practically dissappears for 19 mW excitation as shown in figure 4.2b.
The observed $I_{2\omega}$ can be very well described by:

$$I_{2\omega} = |A_S \exp(i\phi) + A_B \cos 2\psi|^2 \tag{10}$$

The measured curves are fitted to equation 10 with the following three fitting parameters: the interface amplitude A_S, the phase angle ϕ and the bulk amplitude A_B. Both the interface and bulk amplitudes are combinations of intrinsic and field induced terms. From the bias field and power dependences it followed that the bulk contribution A_B is insensitive to changes in the applied voltage and depends linearly on the average pump power, as expected for bulk SHG[6]. We can then normalise the interface amplitude A_S to A_B. From equations 1 and 2 we expect the normalised interface contribution A_S' as a function of V_b to be of the following form:

$$A_S' = C_0 + C_1\sqrt{\Phi_{b0} - V_b} \tag{11}$$

Figure 4.3 shows the bias dependence of A_S' measured with a pulse width of about 100 fs and an average laser power P_ω of 8 mW. The line is a fit, according to Eq. 11 with C_0 and C_1 as fitting parameters. Using formulas from Sze[30] Φ_{b0} is calculated to be equal to 0.8 V. With $C_0 = 0.06$ the fit is in good agreement with our results. C_1 depends on the average power of the incident laser beam.
Figure 4.4 shows the power dependence of A_S' measured at -4 V bias and with a pulsewidth of 100 fs . In this figure it can be seen that A_S' decreases as the average laser power is increased.

These observations can be interpreted in the following way.The pump laser beam will excite charge carriers since the photon energy is above the bandgap of GaAs. Very shortly after excitation a number of holes will reach the top Au contact, where they neutralize the surface charge, leading to a reduced field strength. In the case that the photo- excited charge density exceeds significantly the intrinsic one, the applied field may be totally quenched by only a small part of the excited holes. A similar effect occurs when the holes are collected in front of the AlGaAs barrier where they screen the applied voltage. It will take some time before the field will be restored. Based on the capacitance per area (520 μmF/m^2), the size of the excitation beam (100 μm) and the square resistance of the Au film (a few Ohms), we estimated the RC time constant of this process to be in order of 10 ps. This means that during the laser puls the effective bias is near zero, whereas the system is back to equilibrium before the next puls arrives.
A reduced field strenght results in a lower interface contribution to the $I_{2\omega}$. The lowering of the interface contribution depends on the time between the generation of the carriers and the generation of the SHG signal. In the experiment one pulse generates the carriers and also generates the SHG signal to probe the field. So the time delay between the pump and the probe is of the order of the pulse width. Repeating these experiments with longer excitation pulses already indicated a time dependence of this effective bias. To probe the time evolution of this field dynamics more directly, puls-probe experiments are momentarily in progress. From the results above we may conclude that SHG is indeed sensitive for the Schottky barrier field and as a result SHG can be used to probe the dynamics of this interface field as well. Similar dynamics studies on a semiconductor surface have recently been reported by Dekorsky et al [31] using an ultrafast linear electrooptic technique. This effectively probes the depletion layer, and as such, that technique is complementary to our approach.

5 Summary and future prospects.

In these lectures, it has been shown how a second order nonlinear optical technique like SHG can be used to study the structure, symmetry and electronical structure of semiconductor interfaces. Compared to the ultimate in plane spatial resolution of an STM, SHG can be said to adress two other dimensions: the direction normal to the plane and the time. In addition, the out of plane resolution is not limited to a surface, but can be used to probe buried interfaces, that are hardly accessible otherwise. Yet, an ultimate dream is to combine the superior lateral resolution of an STM with the superior time resolution of a laser. This combination of STM and optics is one of the most exciting recent developments in nanoscopic physics and devices[32, 33, 34, 35]. Also here, nonlinear e.m. phenomena play a crucial role, for example for the mixing of two optical signals via the highly nonlinear $I - V$ characteristic of the tunnel junction. An alternative approach to an optical STM is by using an optically pumped semiconductor tip[36].
Presumabaly, very soon, "4-dimensional" microscopes will be possible!

5.1 Acknowledgements.

Part of the work described here is the result of recent, still unpublished research of our group in Nijmegen. In particular I want to thank C.W. van Hasselt, W. de Jong, A.F. van Etteger and C.A. van 't Hoff. This work was part of the research programme of the Stichting voor Fundamenteel Onderzoek der Materie (FOM) and financially supported by the Nederlandse organisatie voor Wetenschappelijk Onderzoek (NWO).

References

[1] See for instance: Semiconductor Interfaces at the Sub-Nanometer Scale, NATO ASI series E: Applied Sciences Vol. 243; H.W.M. Salemink and M.D. P. Ashley ed.

[2] G. Binnig, H. Rohrer, Ch. Gerber and E. Weibel, Appl.Phys.Lett. **40**, 178 (1982), Phys.Rev.Lett. **49**, 57 (1982).

[3] G. Somerjai, Chemistry in two dimensions: Surfaces (Cornell Univ. Press, N.Y. 1981).

[4] Y.R. Shen, "Surface properties probed by second-harmonic and sum-frequency generation", Nature **337**, 519-525 (1989).

[5] G.L. Richmond, J.M. Robinson and V.L. Shannon, "Second-harmonic generation studies of interfacial structure and dynamics", Prog. Surf. Sci. **28**, 1-70 (1988).

[6] Y.R. Shen, *The Principles of Nonlinear Optics*, Wiley, New York (1984).

[7] T.F. Heinz, M.M.T. Loy and W.A. Thompson, J.Vac.Sci.Technol. **B3**, 1467 (1985).

[8] M. Heusler, Surf.Sci. **36**, 109 (1973).

[9] M.A. Verheyen, C.W. van Hasselt and Th. Rasing, Surf.Sci. **251/252**, 467 (1991).

[10] G.G. Maliaras, H.A. Wierenga and Th. Rasing, Surf.Sci. **287/288**, 703 (1993).

[11] T.F. Heinz, M.M.T. Loy and W.A. Thompson, Phys.Rev.Lett. **54**, 63 (1985).

[12] see for instance: "The Physics and Chemistry of SiO_2 and the $Si-SiO_2$ interface 2", C.R. Helms and B.E. Deal eds., Plenum Press, N.Y. (1993).

[13] H.W.K. Tom, T.F. Heinz and Y.R. Shen, Phys. Rev. Lett. **51**, 1983-1986 (1983).

[14] J.A. Litwin, J.E. Sipe and H.M. van Driel, Phys. Rev. B **31**, 5543-5546 (1985).

[15] D. Guidotti, D.A. Driscoll and H.J. Gerritsen, Solid State Commun. **46**, 337-340 (1983).

[16] R.W.J. Hollering and M. Barmentlo, Optics Commun. **88**, 141-145 (1992).

[17] S.V. Govorkov, N.I. Koroteev, G.I. Petrov, I.L. Shumay and V.V. Yakovlev, Appl. Phys. A **50**, 439-443 (1990).

[18] U. Emmerichs, C. Meyer, K. Leo, H. Kurz, C.H. Bjorkman, C.E. Shearon, Y. Ma, T. Yasuda and G. Lucovsky, Materials Research Science Symposium Proceedings **281**, 815-820 (1992).

[19] O.A. Aktsipetrov, I.M. Baranova and Yu.A. Il'inskii, Sov. Phys. JETP **64**, 167-173 (1986).

[20] J.E. Sipe, D.J. Moss and H.M. van Driel, Phys. Rev. B **35**, 1129-1141 (1987).

[21] M. Born and E. Wolf, *Principles of Optics*, Pergamon, Oxford (1980).

[22] D.S. Bethune, J. Opt. Soc. Am. B **8**, 367-373 (1991).

[23] M.S. Yeganeh, J. Qi, J.P. Culver, A.G. Yodh and M.C. Tamargo, Phys. Rev. B **46**, 1603-1610 (1992).

[24] D.E. Aspnes and A.A. Studna, Phys. Rev. B **27**, 985-1009 (1983).

[25] *Handbook of Optical Constants of Solids*, ed. E.D. Palik, Academic Press, New York (1985).

[26] P.C.M. Christianen, Phd. thesis, University of Nijmegen (1993).

[27] P.C.M. Christianen, P.J. van Hall, H.J.A. Bluyssen and J.H. Wolter, Semicond. Sci. Technol. **9**, 707 (1994).

[28] J. Qi, M.S. Yeganeh, I. Koltover, A.G. Yodh, and W.M. Theis, Phys. Rev. Lett. **71** (1993) 633.

[29] T. Stehlin, M. Feller, P. Guyot-Sionnest and Y.R. Shen, Optics Lett. 13 (1988) 389.

[30] S.M. Sze, Physics of Semiconductor Devices, 2nd ed. (Wiley, New York, 1981).

[31] T. Dekorsky, T. Pfeifer, W. Kütt, and H. Kurz, Phys. Rev. B 47 (1993) 3842.

[32] G. Nunes Jr. and M.R. Freeman, Science **262**, 1029 (1993).

[33] S. Weiss et al., Appl.Phys.Lett. **63**, 2567 (1993)./

[34] M.R. Freeman and G. Nunes Jr., Appl.Phys.Lett. **63**, 2633 (1993).

[35] K. Takeuchi and Y. Kasahara, Appl.Phys.Lett. **63**, 3548 (1993).

[36] M.W.J. Prins, M.C.M.M. van der Wielen, R. Jansen, D.L. Abraham and H. van Kempen, Appl.Phys.Lett. **64**, 1207 (1994).

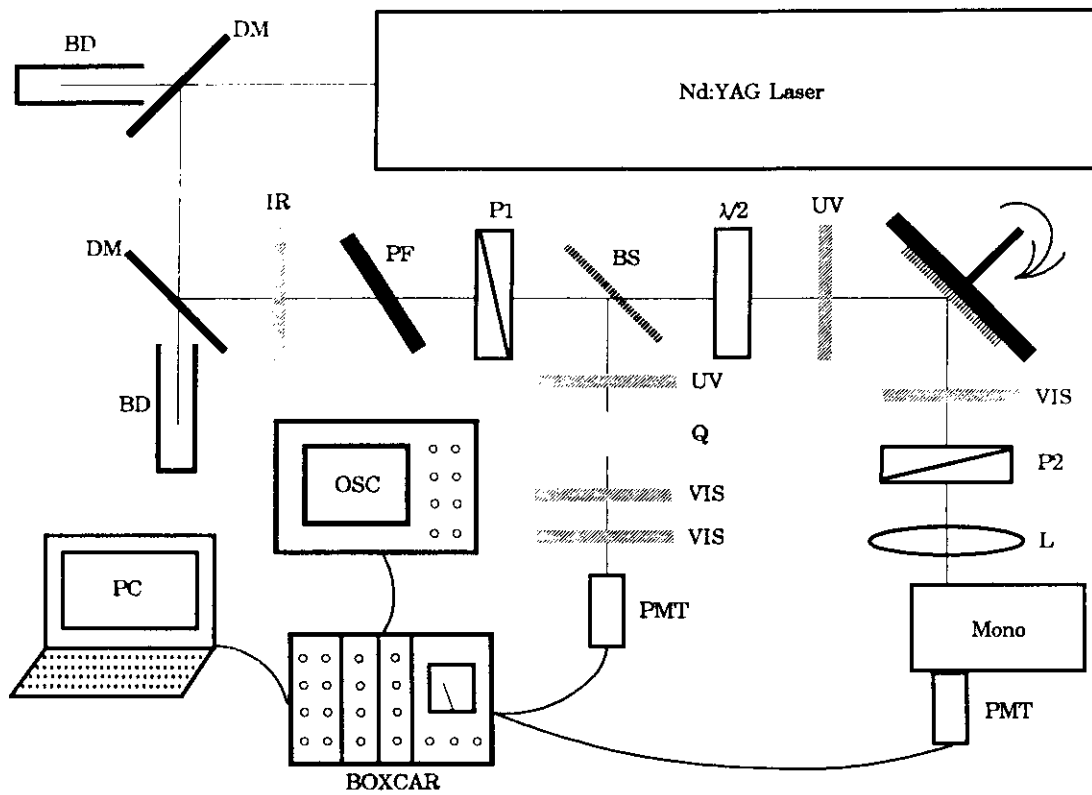

Fig. 1.
SHG experimental setup with dichroic mirrors (DM), beam dumps (BD), filters (IR, VIS, UV), power filter (PF), polarizers (P1, P2), half wave plate ($\lambda/2$), quartz reference sample (Q), photomultipliers (PMT) and gated electronics.

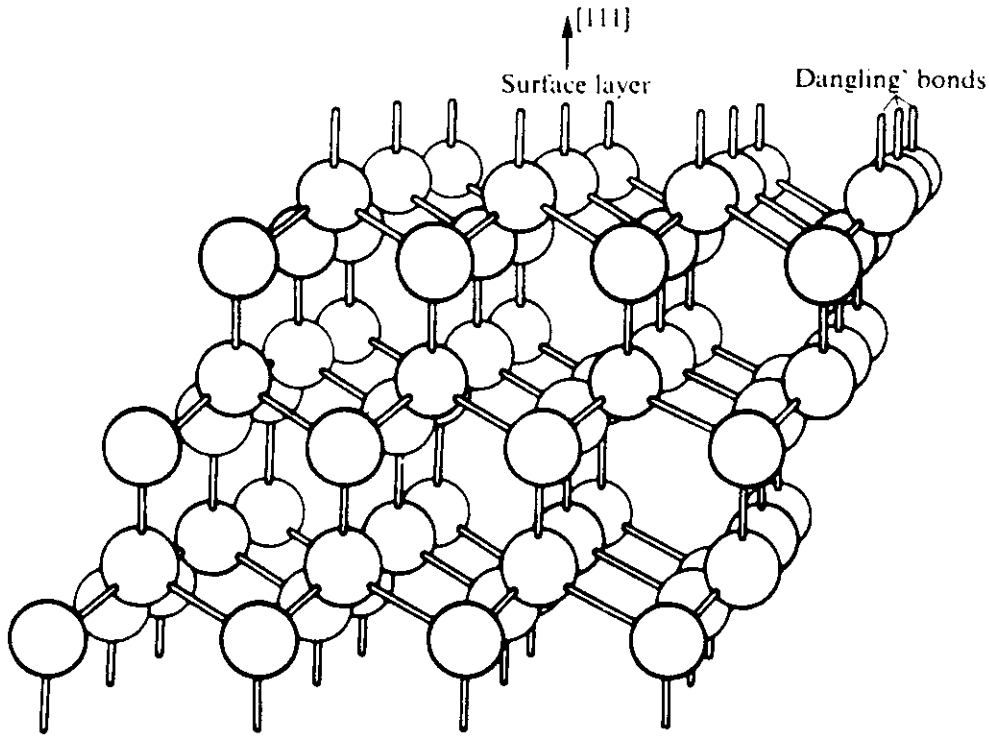

FIG. 1.3. 'Dangling' bonds from the (111) surface of a covalently bonded diamond cubic structure.

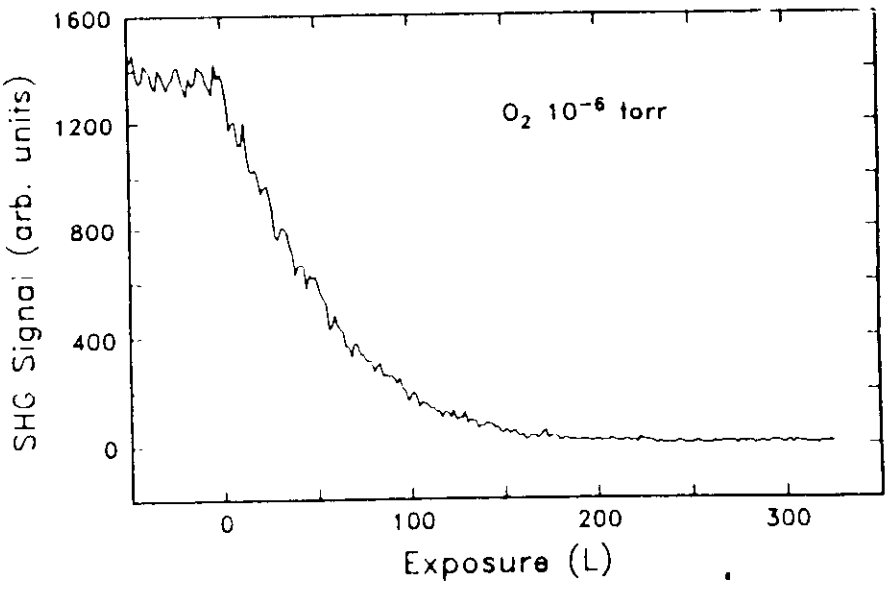

FIG. 1.4 SH intensity from a Si(111)-7 × 7 surface during exposure to oxygen.

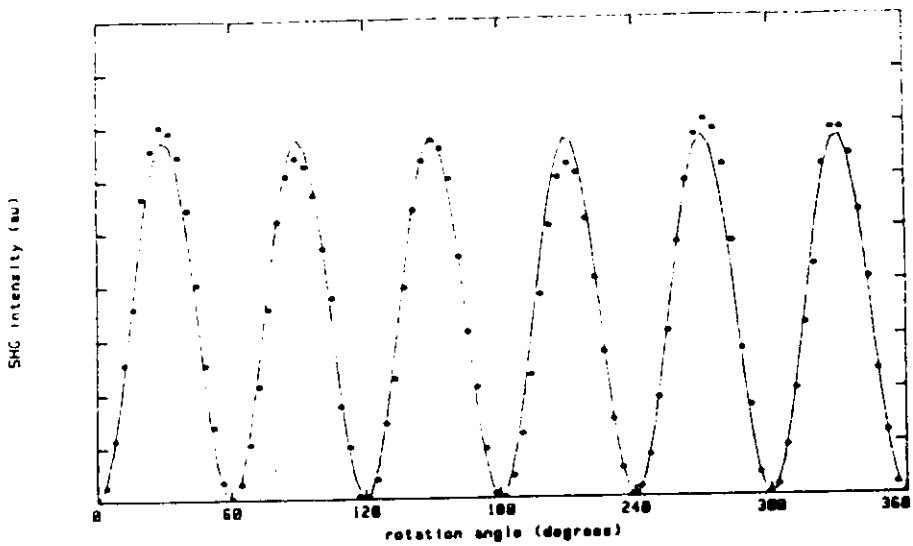

Fig. 1.4 S-polarized SHG intensity for s-polarized pump from Si(111) as a function of the sample rotation angle ϕ.

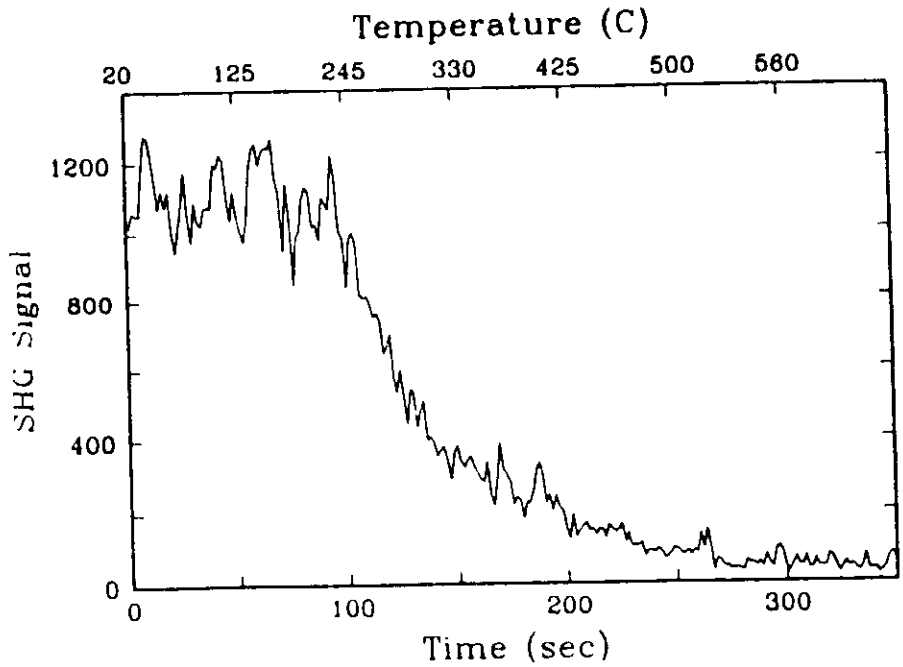

FIG.1.5 SH signal monitoring the establishment of a mirror plane during the 2×1 to 7×7 surface phase transformation. The horizontal axis is calibrated both in elapsed time (below) and in sample temperature (above).

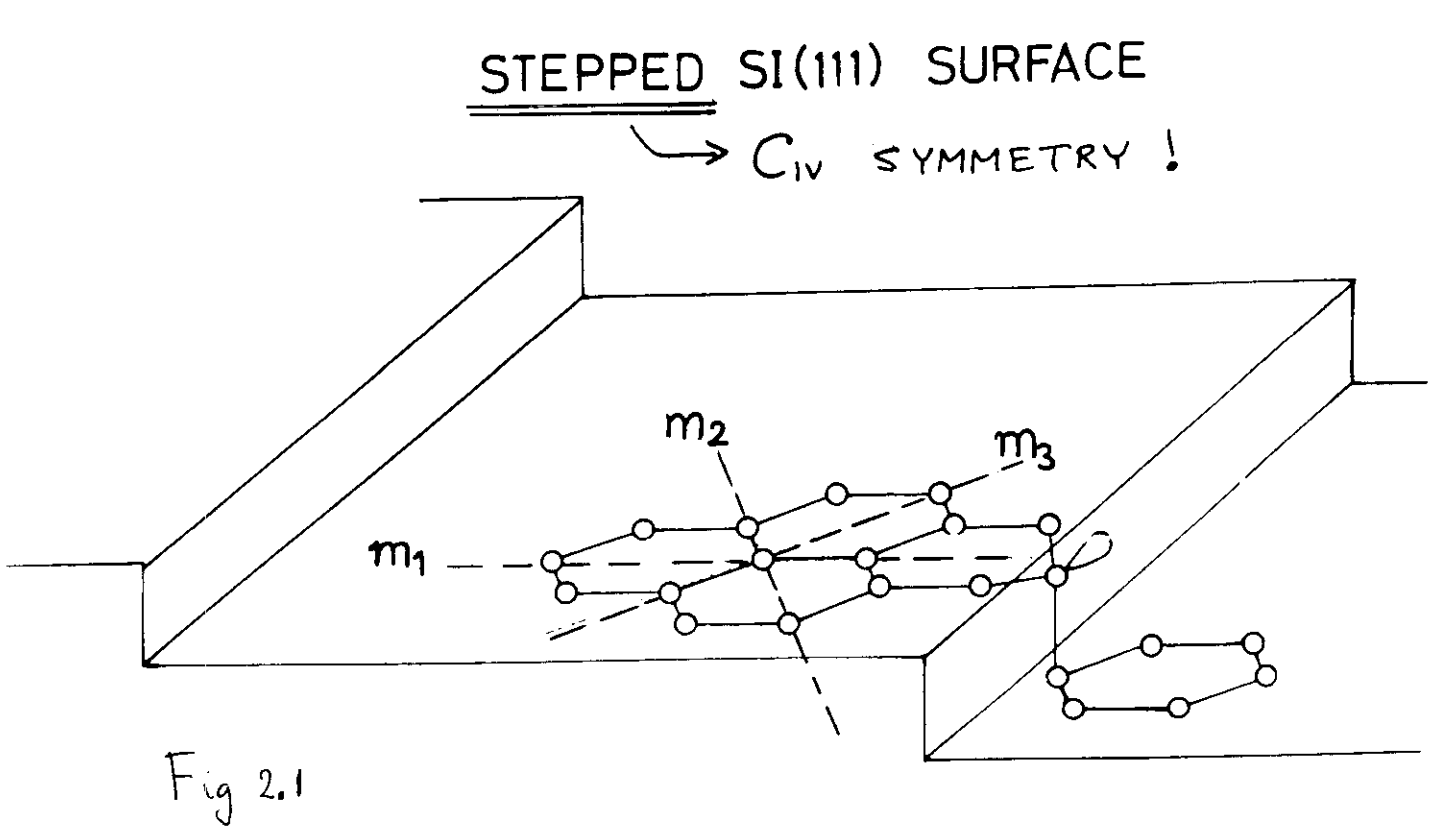

Fig 2.1

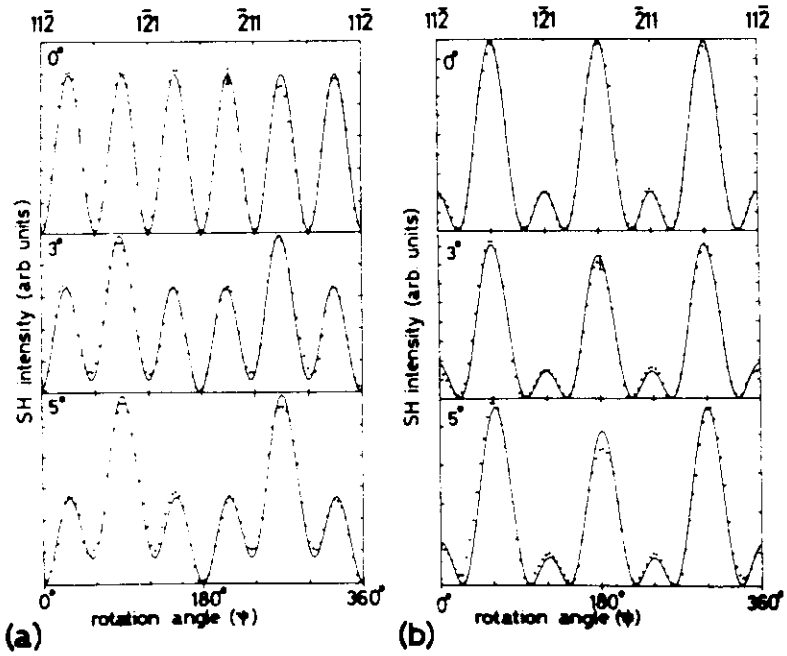

Fig. **2.2** SHG intensity from vicinal Si(111) surfaces as a function of the sample rotation angel ψ for two polarization combinations. (a) s-polarized SHG intensity for s-polarized pump. (b) p-polarized SHG intensity for s-polarized pump. The top traces (0°) show the 3m symmetry, while the results for the two vicinal surfaces (offset angles 3° and 5°) show the interference of 3m and 1m symmetry. The dots are the experimental points, the solid lines a fit.

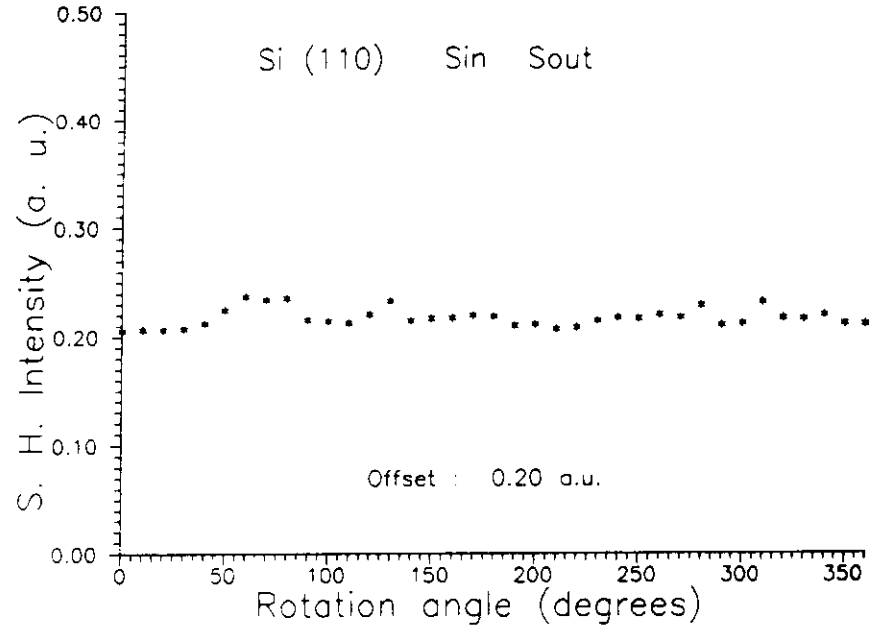

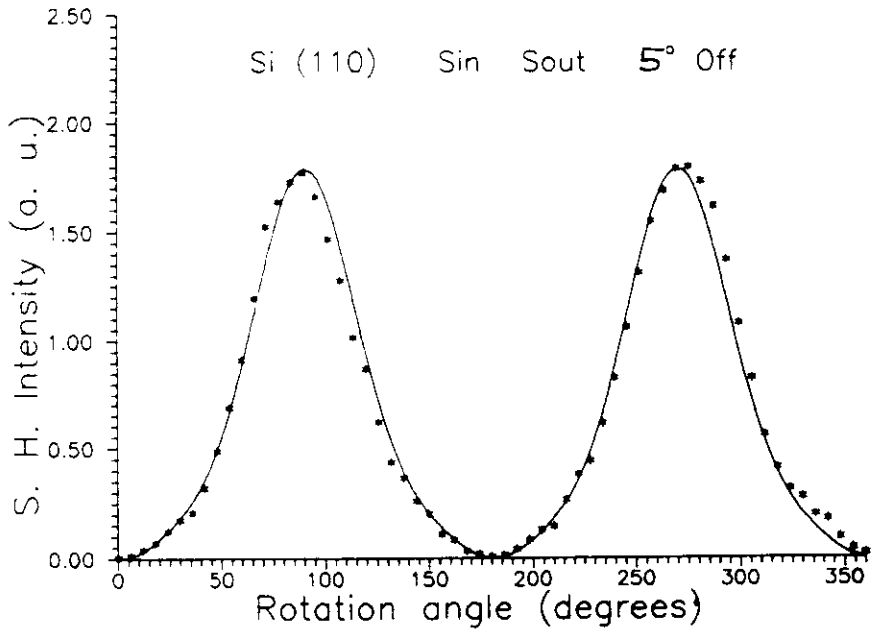

Fig. **2.3** SHG from Si(110) surfaces. (s-in, s-out)

Top: normal, unstepped 110 surface, showing almost negligible SHG (note difference in scale and zero offset !)

Bottom: response of a vicinal 110 surface (5° offset angle), showing strong SHG response with a 1m symmetry.

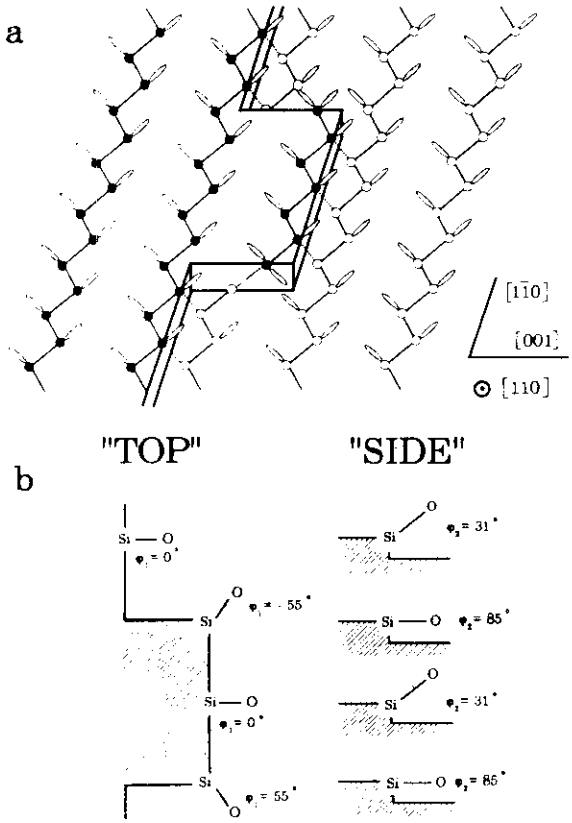

(a) Three-dimensional view of a step, where black and open circles represent Si atoms at different heights (half a unit cell vector). Solid lines represent Si–Si bonds perpendicular to [110], while dashed lines represent bonds between two Si atoms at difference heights. The Si–O bonds are shown as lobes; (b) top and side view of the bonds located at steps and kinks, where the angles are like in the text.

Fig 2.4

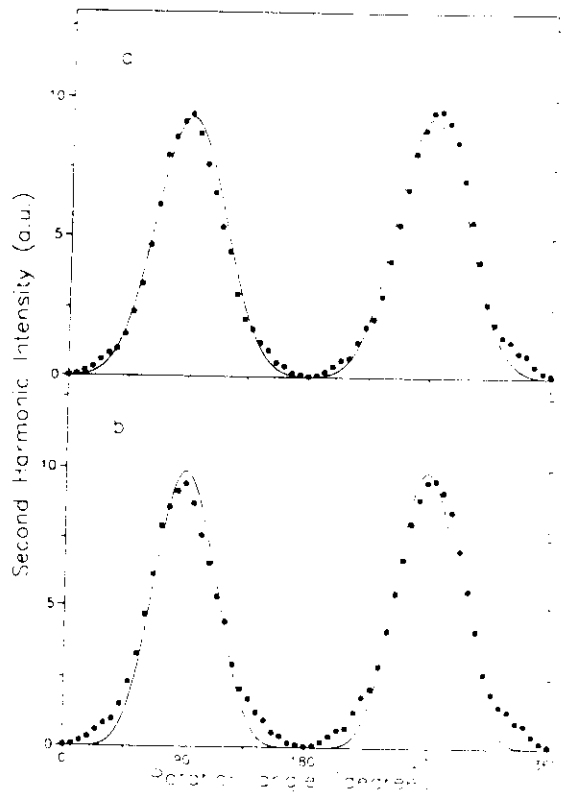

Experimental results from the sample with 5° offset: (a) the solid line is a fit to eq. (6), revealing an x of 4.2%; (b) for the sake of comparison, the solid line is a fit to eq. (6) with no kinks present ($x = 0$).

Fig 2.5

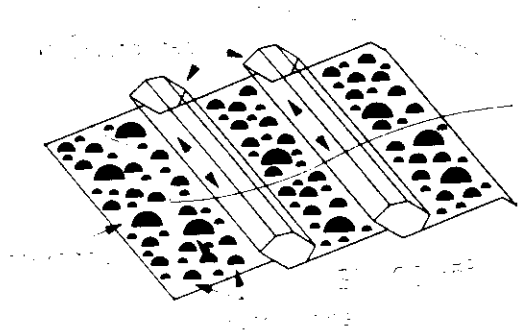

Fig. 3.1
Schematic picture of a $Si - SiO_2$ interface, showing microcrystallites and protrusions.

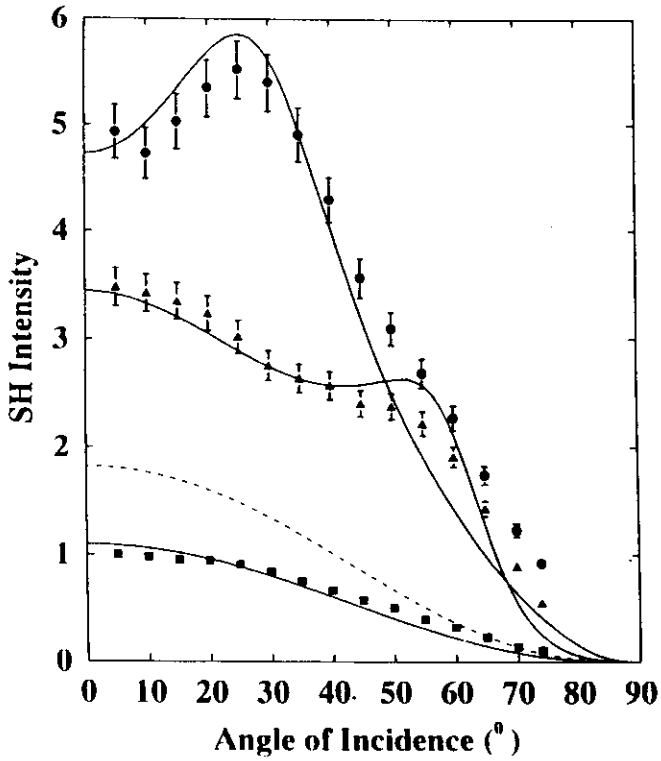

Fig.3.2
Amplitude of $I_{s,s}$ as a function of angle of incidence for oxide thicknesses of 310nm (circles), 260nm (triangles) and 2nm (squares). All measurements have been calibrated to the measurement on the 2nm natural oxide at 4°. The solid lines represent the model, where the scaling parameter is the same for 310nm and 260nm oxide, and the dotted line is the prediction for a 2nm thermal oxide.

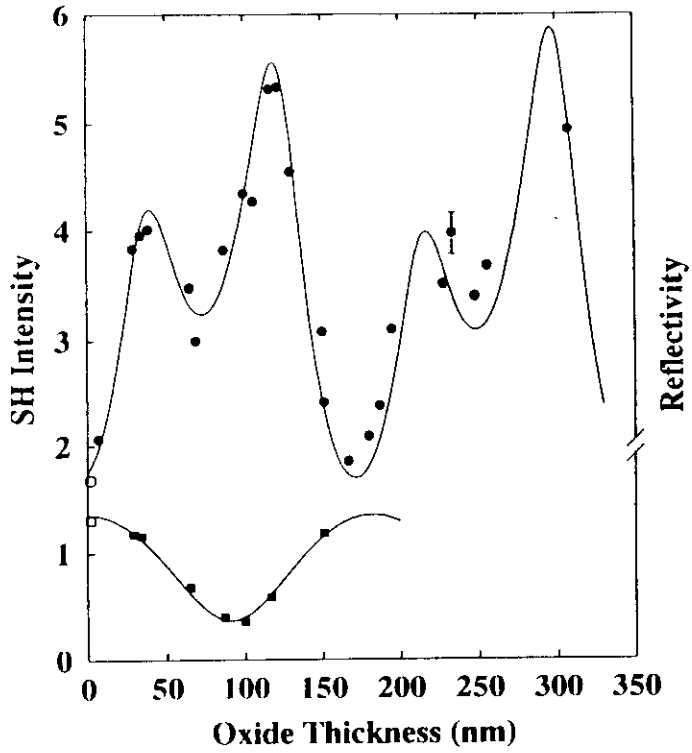

Fig.3.3
Amplitude of $I_{s,s}$ (dots and left vertical axis) and linear reflection (squares and right vertical axis) as a function of oxide thickness for a 4° angle of incidence. The open symbols represent measurements on a part of the sample that was etched clean and then oxidized again. The solid lines are the models for both.

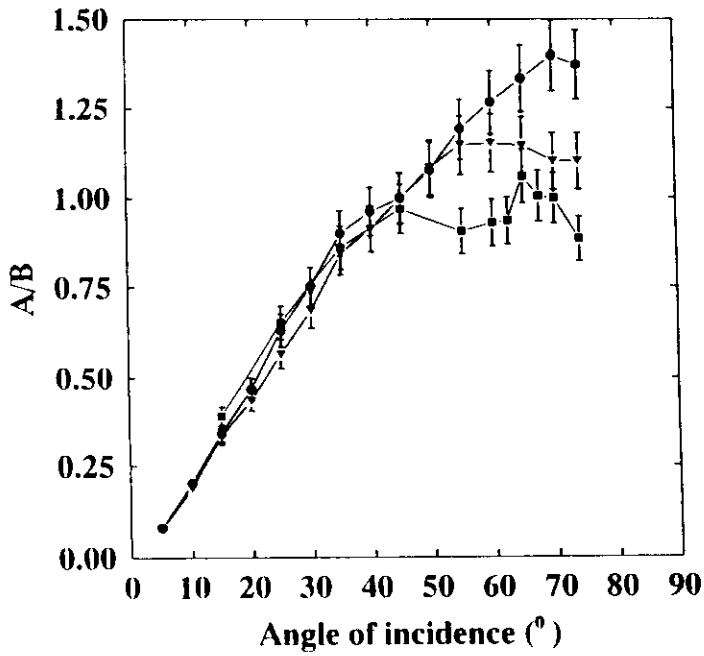

Fig.3.4
Quotient A/B as a function of angle of incidence for oxide thicknesses of 310nm (circles), 260nm (triangles) and 2nm (squares). A is the isotropic and B the anisotropic contribution to $I_{p,p}$. The solid lines are guides to the eye.

Carrier Sweepout of a Schottky Barrier

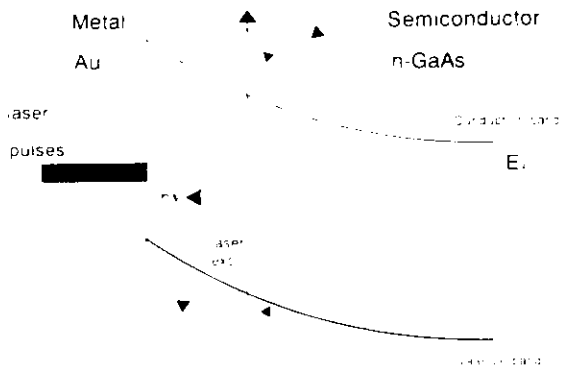

Field: $\sim 10^5$ V cm $^{-1}$ Transit times: $\sim$ 1 ps

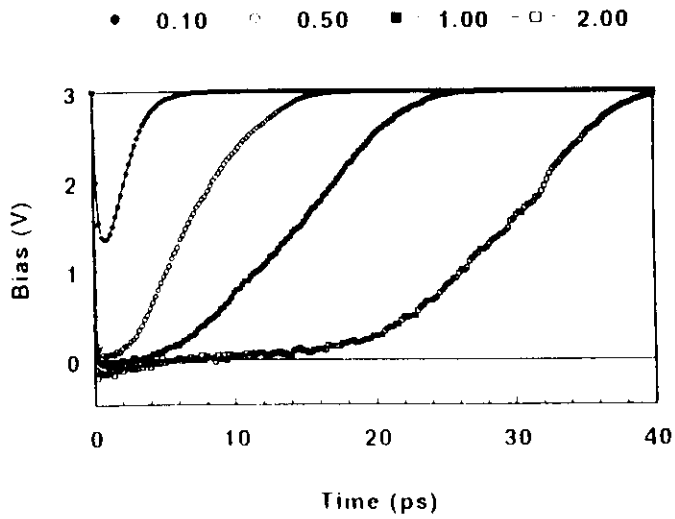

Fig. 4.1
a. Schematic representation of the band bending at a metal-semiconductor interface and the resulting sweepout of the laser excited carriers.
b. Time evolution of the effective bias voltage of 3.0 V and a regeneration time of 1.0 ps for a number of input powers (legens corresponds to input power in mW).

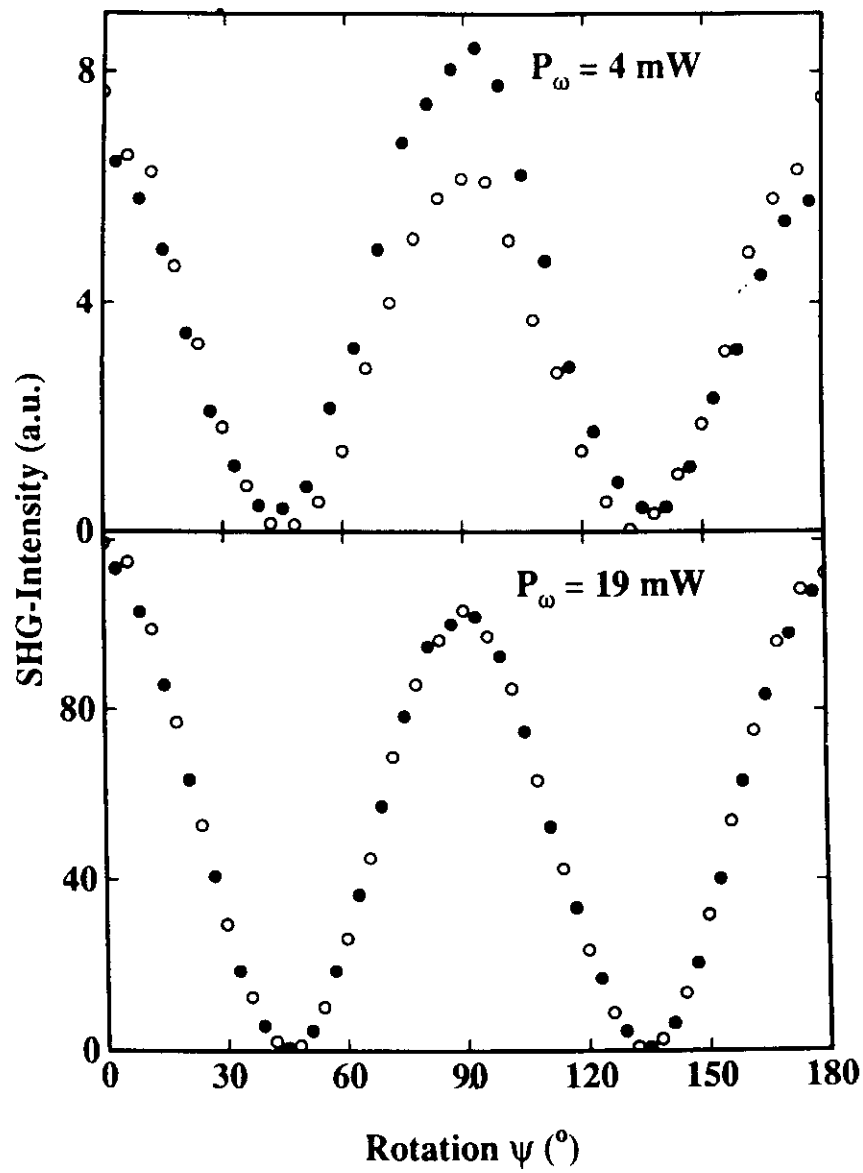

Figure 4.2. a) Azimuthal anisotropy fo the GaAs/Au sample for two different bias voltages, measured with an average laser power of 4 mW and a pulse width of 100 fs. The open circles present data at 0 V bias, the dots at -4 V.
b) The same, measured with an average laser power of 19 mW.

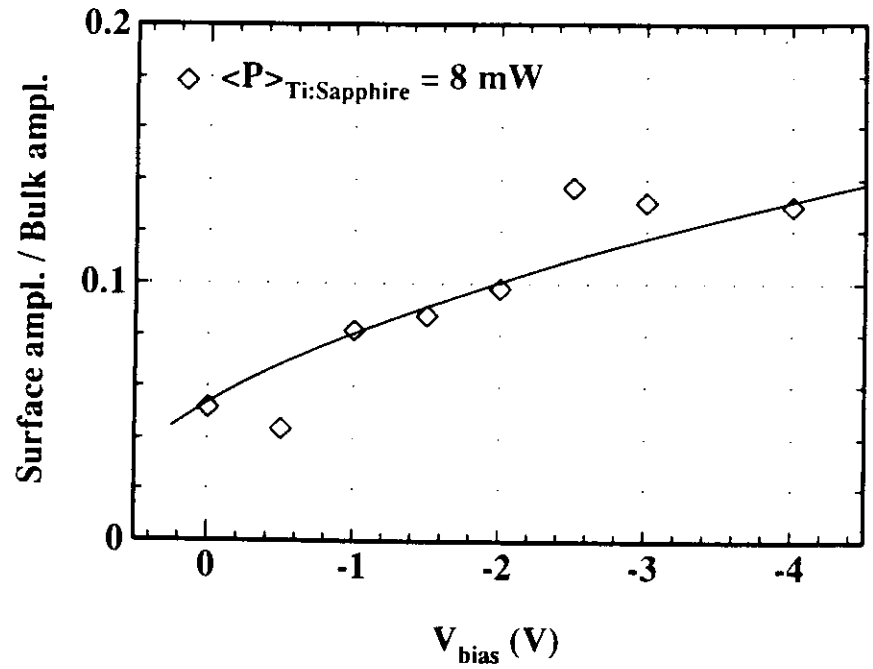

Figure 4.3. Bias dependence of the normalised interface contribution measured with a pulsewidth of 100 fs at an average laser power of 8 mW. The line is a fit according to formula 11.

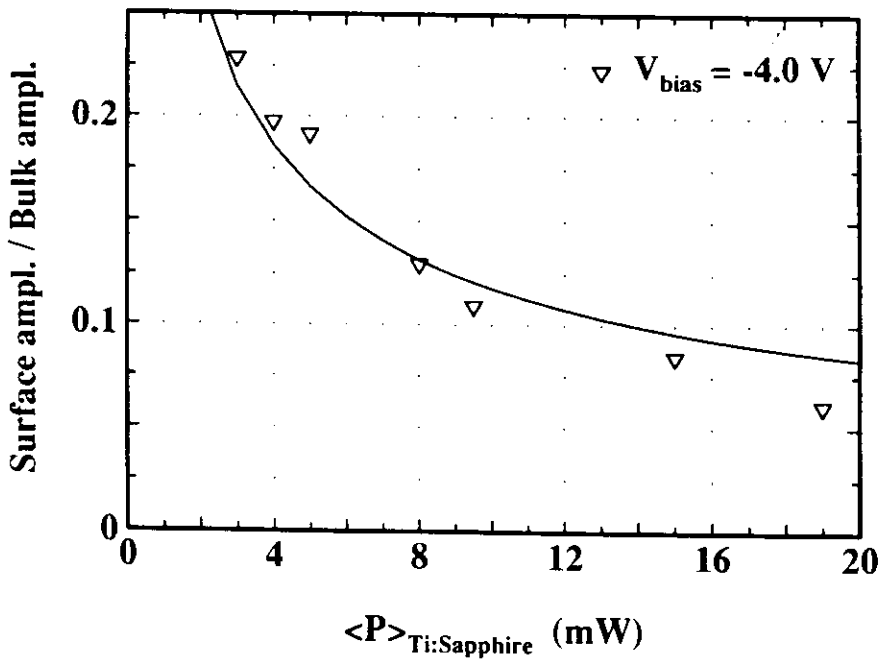

Figure 4.4 Power dependence of the normalised interface contribution measured at -4 V bias with a pulsewidth of 100 fs. The points are connected to guide the eye.